Volume : 3 | Issue : 11 | November 2014 • ISSN No 2277 - 8179

Research Paper

Physical Sciences

KEYWORDS : Cu_2ZnSnS_4; CZTS; chemical deposition; thin film solar cells

Cu_2ZnSnS_4 thin film solar cells

Maarif Jafarov	Baku State University, Baku 1045, Z.Khalilov st.23, Azerbaijan
E.F. Nasirov	Baku State University, Baku 1045, Z.Khalilov st.23, Azerbaijan
S.A.Jahangirova	Baku State University, Baku 1045, Z.Khalilov st.23, Azerbaijan

ABSTRACT

A low-temperature colloid synthesis approach was applied to synthesize Cu_2ZnSnS_4 (CZTS) nanoparticles for the first time. This method produced gram quantities of material with a chemical yield in excess of 90% within a short synthesis time. The formation reaction of kesterite CZTS fabricated from synthesized nanoparticles was investigated, and the results showed that the sufficiently high partial pressures of Sn with S during the annealing process were important for the fabrication of high-quality CZTS films. The compositional ratios as determined by energy-dispersive X-ray spectroscopy (EDX) after the KCN etch are Cu/(Zn,Sn): 1.0 and Zn/Sn: 1.0.

1. INTRODUCTION

The successful development of chalcopyrite-type semiconductors such as $Cu(In,Ga)Se_2$ has led to commercialization by an increasing number of companies. Favorable optoelectronic properties yield efficiencies close to 20% on the single cell and well above 10% on themodule level. Despite or even as a direct consequence of its recent and near-future success, the scarcity and increasing prices of indium eventually could limit the production growth for this type of solar cells. Seeking alternatives not containing indium, the related thin-film material Cu_2ZnSnS_4 (CZTS) shows a very similar crystal structure with a direct band gap expected in the range of 1.4–1.5 eV [1], while containing solely abundant and nontoxic elements. The electrodepostion of CZTSSe thin films can be summarized into two categories: sequential electroplating of precurosors, and single step elctrodeposition of precursors, followed by annealing under sulfur or selenium-containing atmosphere. The first report on CZTS thin films using the sequential deposition approach was who annealed a metal stack of Cu/Sn/Zn (top) deposited on a Mo coated glass substrate at 550 °C for 2 h in sulfur atmosphere. Secondary phase of SnS2 was observed by the XRD measurement in the CZTS thin films. Devices fabricated from such films showed 0.8 % efficiencies.

Ahmed *et al.* [3] developed a three-step method: i) sequentially electroplated Cu/Zn/Sn or Cu/Sn/Zn stacks; ii) annealing the stacks at low temperature (210-350 °C) under N_2 to produce homogeneous alloys; iii) annealing of these well-mixed CuZn and CuSn alloys at 550- 590 °C in sulfur atmosphere for 5-15 min to allow the formation of CZTS. Secondary phases such as Cu_2S, SnS and Cu_2SnS_3 were found in the annealed samples when the annealing temperature lowers than 580 °C. They proposed that secondary phases of ZnS and Cu_2SnS_3 reacted to form CZTS when the annealing temperature was above 580°C. Solar cells made from the CZTS samples prepared from sulfurization of CuZnSn precursors at 585°C for 12 min showed efficiencies ranging from as high as 7.3 %. This is highest efficiencies for the pure CZTS-based solar cells prepared from electrodeposition to date. Recently, Guo *et al.* [5] using a similar deposition process, fabricated 7.0 % efficient CZTS and CZTSe based solar cells. After annealing of the Cu/Zn/Sn metal stacks at 360 °C in N2 for 30 min, the samples sealed in a closing quartz tube together with sulfur or selenium were annealed at 535-585 °C for 5-20 min. The optimized salinization conditions were found to be at 585°C for 7 min while the optimized sulfurization conditions were at 585 °C for 12 min. They proposed that the low shunt resistance in CZTSe-based solar cells (0.48 KΩcm^2) in contrast to CZTS-based solar cells (11.8 KΩcm2) is due to the existence of a Se-poor and Sn-rich grain boundary region. They also proposed that the oxygen observed in the CZTS/CZTSe thin films may be responsible for the low JSC in the corresponding devices.

Co-electrodeposition of Cu-Zn-Sn precursors for CZTS thin films was introduced for the first time by Ennaoui *et al.* [6]. They deposited Cu-Zn-Sn precursor layers on the Mo coated soda lime glass substrate from alkaline electrolyte bath containing Cu (II), Zn (II), and Sn (IV) metal salts in a single step. The precursor layers annealed 550 °C in Ar-H2S (5 %) atmosphere for 2h to allow the reaction of the precursors to form CZTS. EDX mapping analysis revealed existence of an area with reduced Zn signal near the back contact, which may point to Cu2SnS3 phase. Solar cells fabricated from CZTS films with Cu/(Zn + Sn) = 0.97 and Zn/Sn = 1.08 showed an efficiency of 3.4 %. Using a similar co-electrodeposition process, Araki *et al.* [7] reported 3.16 % efficient CZTS-based thin films solar cells. The sulfurization of the Cu-Zn-Sn precursor layers was performed at higher temperature (580 or 600 °C) compared to that reported by Ennaoui *et al.* (540 °C) [8] for the same time (2 h). Sample annealed at 600 °C gave the best solar cells.

2. EXPERIMENTAL

Alluminium and indium tin oxide (ITO) glass slides were used as the substrate during the deposition process polycrystalline CZTS thin films. The substrates were first cleaned in ethanol then ultrasonically washed with distilled water. Finally, substrates were dried in an oven at 90°C. In the typical synthesis, CuCl (1mmol), $ZnCl_2$ (0.75 mmol), and $SnCl_2$ (0.6mmol) were added into pyridine as a metal source and the Cu/Zn/Sn molar ratio was determined to be 2/1.5/1.2. The mixture was cooled to 0^{0}C with stirring until the mixture turned into a clear solution and then purged with argon. Then, 25 mL of sodium selenite (0.15 M) was added and the pH of the solution was adjusted to 3 by addition of hydrochloric acid using pH meter. Na_2S (1.85 mmol) dissolved in methanol, were applied as chalcogenide sources to fabricate Cu_2ZnSnS_4 (CZTS), nanoparticles, as shown in reaction formulas (1).

$$2CuCl_2 + 1{,}5ZnCl_2 + 1{,}2SnCl_2 + 3{,}7Na_2S_2O_3 \rightarrow Cu_2Zn_{1.5}Sn_{1.2}S_{3.7} + 7{,}4NaCl \quad (1)$$

The methanol solutions of Na_2S were also purged with argon and cooled to 0^{0}C, respectively, followed by a quick transfer into the metal sources to react with CuCl, $ZnCl_2$, and $SnCl_2$ for 2 min. The products were centrifuged and washed with organic solvent three times to remove the byproduct of NaCl. Finally, the products were dispersed into organic solvents by sonication for 20 min. No nanoparticles were observed when Na_2S was used as the chalcogenide source. In contrast, the nanoparticles were detected when Na_2S was used as the chalcogenide source. However, it was found that the particle size distribution was wide. When Na_2S were used as the chalcogenide sources, the synthesized nanoparticles showed a narrow diameter distribution, suggesting

Volume : 3 | Issue : 11 | November 2014 • ISSN No 2277 - 8179

that they are the optimum chalcogenide sources for the fabrication of nanoparticles in our case. It is obvious that the chalcogenide source affects the results of the synthesis reaction. The possible reason for this is the different nucleation and growth speeds caused by the different chalcogenide sources. The nucleation speed was fast and it resulted in the formation of numerous small nuclei when Na_2S was used. The small nuclei quickly agglomerated together by van der Waals attractive forces and grew into a big bulk, causing no nanoparticles to be detected. The slow nucleation speed caused growth of nuclei, which occurred with nucleation at the same time, resulting in the wide range of nucleus size when Na_2S was used as the chalcogenide source. Therefore, the size of CZTS nanoparticles, which grew from the nuclei, shows a wide distribution range. The appropriate nucleation and growth speeds with Na_2S were applied at the same time, resulting in a narrow distribution of diameter, and the average size of the nanoparticles was about 80 nm. The composition of the CZTS nanoparticles as-synthesized for 2 min was confirmed by Energy-dispersive X-ray spectroscopy (EDS). The yields of the CZTS nanoparticles exceeded 90%, which was determined after the evaporation treatment of the solvent. No diffraction peaks were observed in the XRD results (data not shown), suggesting that the CZTS nanoparticles were almost amorphous materials. The CZTS nanoparticles were coated on Al substrates followed by drying and partial decomposition on a preheated hot plate. Annealing treatment has been performed to improve the crystallinity of the films in a quartz box with a volume of 16 cm^3 at various temperatures for 60 min. of kesterite CZTS.

Figure 1 shows the XRD patterns of the CZTS films annealed for 60 min. For the sample annealed at 450^{0}C, the peaks that can be assigned to the kesterite structure were observed, showing that the CZTS crystals were successfully synthesized by this approach.

The intensity of the peaks increased when the annealing temperature up from 400 to 450^{0}C, indicating the improvement of film crystallinity. It was found that the peaks different from those assigned to the kesterite structure started to appear at the annealing temperature of 425^{0}C. The phases assigned from these peaks, which are different from those assigned to the kesterite structure, were considered as possible ZnSe phases at 425^{0}C and SnS with Cu_2Se phases at 450^{0}C The increase of the CZTS peak intensity confirmed the improvement of crystallinity, which is similar to the XRD results. The low-energy shift in the CZTS peak and the decrease of the CZTS peak intensity were observed with increasing annealing temperature from 450 to 500^{0}C, indicating the substitution of S by Se during the annealing process. It is suggested that the CZTS structure entirely decomposed to ZnS, SnS, and $Cu_{2-x}S$ at 500^{0}C. Our results indicate that the CZTS structure was unstable at high temperature, and also easily decomposed even under atmospheric pressure.

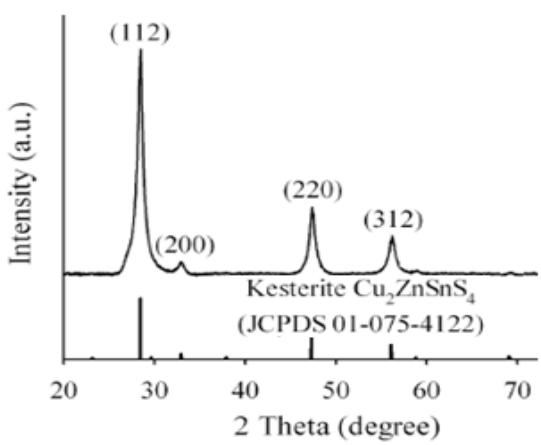

Figure 1. XRD patterns of CZTS film.

In the typical synthesis CdZnS nanoparticles, $CdCl_2$ (0.9mmol), $ZnCl_2$ (0.75 mmol) and $Na_2S_2O_3$ (0.6mmol) were added into pyridine as a metal source and the Cd/Zn/S molar ratio was determined to be 2/1.5/1.2. It is because the devices show high efficiency with a Zn-rich composition, which has been reported. The mixture was cooled to 0^{0}C with stirring until the mixture turned into a clear solution and then purged with argon. The methanol solutions of $Na_2S_2O_3$ were also purged with argon and cooled to 0^{0}C, respectively, followed by a quick transfer into the metal sources to react with $CdCl_2$ and $ZnCl_2$ $InCl_3$ for 2 min. The products were centrifuged and washed with organic solvent three times to remove the byproduct of NaCl. Finally, the products were dispersed into organic solvents by sonication for 20 min. The J–V characteristics of solar cells under illumination were measured with a solar simulator under standard test conditions without light soaking. External quantum efficiencies were analyzed using monochromatic illumination under short-circuit conditions.

3. RESULTS AND DISCUSSION

The scanning electron microscope (SEM) image of a crosssection of the as-deposited kesterite absorber layer is depicted in Figure 2. It shows a relatively homogeneous film all the way from the back contact to the top surface, with no apparent secondary phases. A small contrast change at the top surface might indicate a thin CuS-layer which is typically found for copper-rich growth conditions in chalcopyrite thin-film deposition. This has been checked by GIXRD analysis shown in Figure 2. The Bragg peaks in the diffraction pattern indeed indicate two types of crystal structures, one can be attributed to CZTS (kesterite, tetragonal, Inorganic Crystal Structure and the other one to CuS (covellite, hexagonal). From the GIXRD analysis alone, it is not possible to exclude the occurrence of additional secondary phases, because the Bragg peaks of Cu_2SnS_3 and ZnS could be hidden under the observed kesterite and covellite peaks due to the close relations between the structures of these compounds. The elemental composition has been checked by EDX analysis A Cu/(Zn,Sn) ratio of 1.4 and a Zn/Sn of 1 was determined for the as-grown films.

It can be seen that the copper, zinc, tin, and sulfur concentrations stay constant within the accuracy of the measurement, as indicated by the almost constant net counts of the four elements over the depth of the sample. No particular layering as observed in earlier sequential evaporation experiments is visible. The net counts only give qualitative information about the depth distribution not about the chemical composition. As the energy levels of sulfur K-line and L-line overlap an apparent residual Mo signal from the back contact is detected throughout the absorber. From the GIXRD measurement, the spatial uniformity, the stoichiometric chemical composition and the constant Zn/Sn before and after KCN etching, we exclude significant amounts of secondary phases in the as-grown films other than CuS.

The somewhat porous morphology of the layer likely results from the etching of CuS-secondary phases which covered and enclosed the CZTS crystallites in the as-grown film.

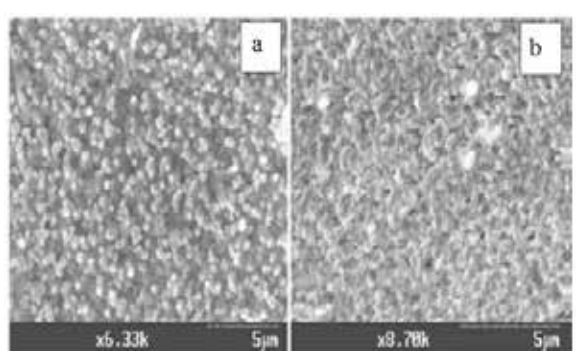

Figure 2. SEM image of the surface of the CZTS absorber be-

fore (a) and after (b) KCN etching

This solar cell device configuration has been developed and used for CdZnS-based solar cells and modules and has not been specifically optimized for the CZTS absorber layers. Figure 3 depicts the J–V characteristics of the best device measured at standard test conditions. This device showed a total area efficiency of 8.0% with an open-circuit voltage of 640mV, a short-circuit current density of 28.0mA/cm^2, and fill factor of 65.8%.

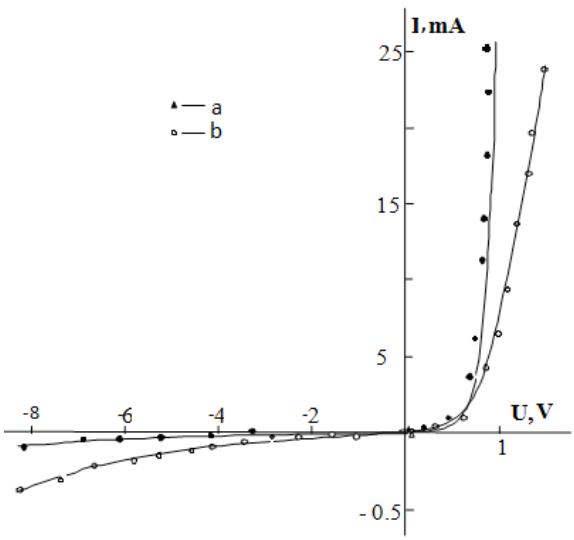

Figure 3. J–V characteristics of solar cell with CZTS absorber, before (a) and after (b)

KCN etching

To gain further insights in the device performance and loss mechanisms the external quantum efficiency (EQE) was measured on the same solar cell as shown in Figure 4. The EQE shows a steep increase around 350 nm related to the absorption edge of the ZnS window layer, a maximum value of about 70% at wavelengths between 400 and 500 nm and a subsequent broad decline for wavelengths above 520 nm (Fig.4). The optical gap of the CZTS absorber layer can be estimated from this EQE measurement, if the absorption coefficient for the material is modeled assuming a direct band gap semiconductor with parabolic bands close to the band edge. For wavelengths larger than the estimated optical gap (820 nm) significant photocurrent collection is observed in the EQE. This is likely due to substantial band tailing due to large amount of lattice disorder in the CZTS film. The collection length can be estimated by analyzing the electrical characteristics of the Al/CZTS/ZnCdS/ZnS structure. Using material parameters consistent with those commonly used for device simulation of Cu(In, Ga)Se_2 or $CuInS_2$ solar cells [8], the J–V and EQE characteristics can be qualitatively reproduced by assuming a bulk diffusion length below 150 nm corresponding to a density of recombination centers in the range of $10^{18}cm^{-3}$, and a space charge width of around 180 nm, corresponding to a net acceptor level of about $2.10^{16}cm^{-3}$.

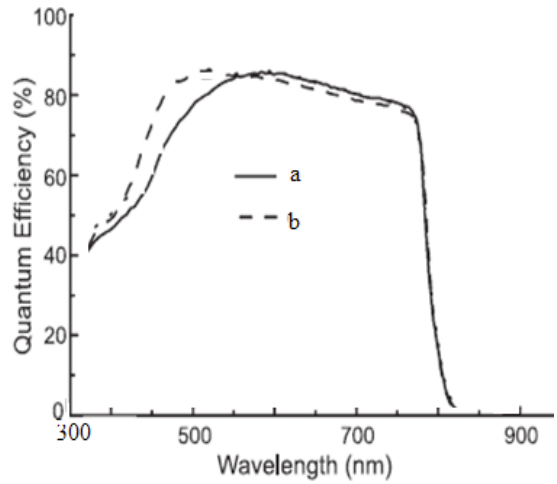

Figure 4. External quantum efficiency (EQE) of solar cell with CZTS absorber, before (a) and after (b) KCN etching.

4. CONCLUSIONS

It has been shown that near-stoichiometric single-phased polycrystalline CZTS thin films can be prepared by a fast deposition process. Copper-rich growth conditions lead to the segregation of a CuS secondary phase which can be removed by KCN etching. Solar cell devices made from these CZTS layers show the currently highest device performance of CZTS based thin film solar cells fabricated by a fast deposition process with a maxi-

REFERENCE

1. B. A. Schubert, B. Marsen, S. Cinque, T. Unold, R. Klenk, S. Schorr, and H. W. Schock: Prog. Photovoltaics 19 (2011) 93. | 2. H. Katagiri, K. Jimbo, W. S. Maw, K. Oishi, M. Yamazaki, H. Araki, and A. Takeuchi: Thin Solid Films 517 (2009) 2455. | 3. K. Maeda, K. Tanaka, Y. Nakano, and H. Uchiki: Jpn. J. Appl. Phys. 50 (2011) 05FB08. | 4. Q. Guo, G. M. Ford, W. C. Yang, B. C. Walker, E. A. Stach, H. W. Hillhouse, and R. Agrawal: J. Am. Chem. Soc. 132 (2010) 17384. | 5. Yang, D.; Zhao, J.; Liu, H.; Zheng, Z.; Adebajo, M. O.; Wang, H.; Liu, X.; Zhang, H.; Zhao, J.-c.; Bell, J.; Zhu, H. Chem.–Eur. J. 2013, 19,5113–5119. | 6. Todorov, T. K.; Tang, J.; Bag, S.; Gunawan, O.; Gokmen, T.; Zhu, Y.; Mitzi, D. B. Adv. Energy Mater. 2013, 3, 34–38. | 7. Regulacio, M. D.; Ye, C.; Lim, S. H.; Bosman, M.; Ye, E.; Chen, S.; Xu, Q.-H.; Han, M.-Y. Chem.–Eur. J. 2012, 18, 3127–3131. | 8. Scragg, J. J.; Dale, P. J.; Peter, L. M.; Zoppi, G.; Forbes, I. Phys. Status Solidi B 2008, 245, 1772–1778. |